Biochimica et Biophysica Acta 1808 (2011) 2761–2771

Contents lists available at ScienceDirect

Biochimica et Biophysica Acta

journal homepage: www.elsevier.com/locate/bbamem

Fluid phase lipid areas and bilayer thicknesses of commonly used phosphatidylcholines as a function of temperature

Norbert Kučerka [a,b,*], Mu-Ping Nieh [c], John Katsaras [a,d]

[a] Canadian Neutron Beam Centre, National Research Council, Chalk River, Ontario, Canada K0J 1J0
[b] Department of Physical Chemistry of Drugs, Faculty of Pharmacy, Comenius University, Odbojárov 10, 832 32 Bratislava, Slovakia
[c] Department of Chemical, Materials & Biomolecular Engineering, Institute of Materials Science, University of Connecticut, Storrs, CT 06269, USA
[d] Neutron Scattering Science Division, Oak Ridge National Laboratory, Oak Ridge, TN, 37831-6100, USA

ARTICLE INFO

Article history:
Received 6 June 2011
Received in revised form 14 July 2011
Accepted 15 July 2011
Available online 23 July 2011

Keywords:
Area per lipid
Bilayer structure
Fluid phase
Neutron scattering
X-ray scattering
Phosphatidylcholine

ABSTRACT

The structural parameters of fluid phase bilayers composed of phosphatidylcholines with fully saturated, mixed, and branched fatty acid chains, at several temperatures, have been determined by simultaneously analyzing small-angle neutron and X-ray scattering data. Bilayer parameters, such as area per lipid and overall bilayer thickness have been obtained in conjunction with intrabilayer structural parameters (e.g. hydrocarbon region thickness). The results have allowed us to assess the effect of temperature and hydrocarbon chain composition on bilayer structure. For example, we found that for all lipids there is, not surprisingly, an increase in fatty acid chain trans–gauche isomerization with increasing temperature. Moreover, this increase in trans–gauche isomerization scales with fatty acid chain length in mixed chain lipids. However, in the case of lipids with saturated fatty acid chains, trans–gauche isomerization is increasingly tempered by attractive chain–chain van der Waals interactions with increasing chain length. Finally, our results confirm a strong dependence of lipid chain dynamics as a function of double bond position along fatty acid chains.

1. Introduction

Throughout the biological world cell membranes are crucial to life. In the case of animal cells the plasma membrane, which is composed predominantly of proteins and lipids, and separates the cytosol from the cell's extracellular environment, acts as a selective semi-permeable barrier. Membranes also surround the various cell organelles (e.g. mitochondria, endoplasmic reticulum, Golgi apparatus, etc.), thus enabling them to maintain their characteristic functions.

The transport of molecules and the chemical signaling processes taking place across the membrane's lipid bilayer are, for the most part, mediated by membrane proteins, while their function (i.e. proteins) is determined by the lipid bilayer's structural properties. It is now generally accepted that the function, insertion, orientation, and subcellular localization of integral membrane proteins are all affected by the membrane's physical properties [1]. An example is the relationship between the activity of integral membrane proteins, such as the sarcoplasmic reticulum Ca^{2+}-transporting ATPase, and bilayer thickness [2]. In this case, enzymatic activity was found to be maximal in bilayers composed of medium length (18-carbon) hydrocarbon chain lipids, and decreased by as much as a factor of four in both short- (14-carbon) and long-chain (22-carbon) lipid bilayers [3].

There are various definitions of lipid bilayer thickness given in the literature, many of which depend on the technique used to measure the thickness, and the physical phenomenon being studied. For example, hydrophobic thickness (D_C) is widely used in cases where the function of an integral membrane protein is affected by hydrophobic mismatch [4]. This thickness is typically defined by the bilayer's hydrocarbon acyl chains and is assumed to be free of water. On the other hand, some amount of water molecules (n_W) is known to intercalate into the lipid headgroup region [5]. The thickness associated with this region (D_H) depends on headgroup conformation, which can be affected by other parts of the bilayer [6], and/or thermodynamic conditions [7]. D_H is also often arbitrarily defined in terms of steric thickness [7–10].

Bilayer thickness can be conveniently determined by various X-ray and neutron scattering experiments — note however, that the two techniques are sensitive to different bilayer thicknesses. In neutron scattering the high contrast between the protonated lipid and the deuterated water defines the overall bilayer thickness (D_B), also known as the Luzzati thickness [11]. On the other hand, the thickness best resolved by X-ray scattering is the distance between the peaks in the electron density (ED) profile, which, for the most part, corresponds to the distance between the lipid headgroup phosphates (D_{HH}). Even though they are the two most robust experimentally determined parameters, D_{HH} and D_B cannot be directly compared to

* Corresponding author at: Canadian Neutron Beam Centre, National Research Council, Chalk River, Ontario, Canada K0J 1J0. Tel.: +1 613 584 8811x44195; fax: +1 613 584 4040.
E-mail address: Norbert.Kucerka@nrc.gc.ca (N. Kučerka).

0005-2736/$ – see front matter.
doi:10.1016/j.bbamem.2011.07.022

each other, and neither provides all of the desired information regarding bilayer structure. Instead, in combination with experimental data, models are used to determine the remaining bilayer structural parameters.

Recently, the scattering density profile (SDP) model that simultaneously fits X-ray and neutron small-angle scattering data has permitted the robust determination of bilayer structural parameters [12]. Even though the primary information obtained from scattering experiments is the various bilayer thicknesses, the SDP model associates them by a common structural quantity that is central to describing bilayer structure — as well as lipid–lipid and lipid–protein interactions — namely the area per lipid along the surface of the bilayer (A). All thicknesses are then related to A through volume considerations (e.g. $A = 2V_L/D_B = (V_L - V_{HL})/D_C = (V_{HL} + n_W V_W)/D_H$, where V_L is the volume of a lipid molecule, V_{HL} is the lipid headgroup volume, and V_W is the volume of a water molecule). It should be stressed that A is not easily determined for fluid lipid bilayers and is only obtainable if additional information is provided to constrain the many parameters that are needed by any realistic model of a bilayer. It should also be emphasized that this is not a criticism for the use of models. On the contrary, the unique advantage of models is that information obtained from different experiments can be used to refine them [13]. For example, total lipid volume is accurately obtained by other techniques [14–16] and is used in our analysis in order to reduce the number of variable parameters.

Accurately known lipid areas are crucial when assessing intermolecular interactions taking place within biomembranes. Historically, for example, models describing the structure of the red blood cell membrane were derived from knowledge of the total area occupied by the membrane's lipids [17]. The complex structural dynamics found in membranes involve a balance of forces, where area is the product of these forces in the lateral direction (i.e. in-plane). In single component lipid bilayers water permeability has been shown to correlate most strongly with area/lipid, but not so well with bilayer thickness and the bilayer's other structural and mechanical properties [18]. As a result, a new model for how water permeates a lipid bilayer was proposed, whereby lipid area was the key determinant [19]. Furthermore, if protein function involves a conformational transition accompanied by a change in its cross-sectional area, it can be assumed that even small changes in membrane lateral pressure (i.e. change in lipid area) can induce significant conformational (i.e. function) changes to a protein [20].

In addition to playing a key role in describing membrane structure and function, knowledge of lateral lipid area is central to simulations [13]. Recent studies suggest that the force fields utilized in molecular dynamics (MD) simulations, however carefully determined may result in poor agreement with experiment when simulations are performed at the ideal zero surface tension condition [21]. To counter this, an alternative approach is to carry out simulations at constant, but nonzero tension, or equivalently at a fixed surface area [13]. The question then becomes, what value should the area/lipid be fixed to? Inconsistencies in lipid areas have been highlighted by the disparate results arising from MD simulations utilizing different force fields. For example, MD simulations based on the CHARMM (Chemistry at HARvard Molecular Mechanics) potentials are performed at nonzero surface tension in order to make them "better agree" with X-ray scattering data [13], whereas simulations using a combination of GROMOS and OPLS (Optimized Potential for Liquid Simulations) potentials do not seem to require this additional "tweaking" [22]. Since MD force fields are considered to be "well tuned" if they are able to reproduce experimental data [23], it is obvious that more work is needed to reconcile simulation and experiment, even in the simplest case of single component membranes.

Due to its complexity, the physical properties and functional roles of individual lipid species in biomembranes are exceedingly difficult to ascertain in an intact membrane. In order to gain insight into the roles of individual components, it is necessary to study model membrane systems that contain the lipid species of interest. For example, in eukaryotic membranes the predominant lipid species is glycerol-based phospholipids, including phosphatidylcholine (PC), phosphatidylethanolamine (PE), phosphatidylserine (PS), phosphatidylinositol, and cardiolipin. In the case of glycerol-based lipids, it is usual to find a saturated fatty acid esterified at the 1-position of the glycerol backbone and an unsaturated fatty acid at the 2-position. Also, compared to other lipids PE and PS lipids contain fatty acid chains with a greater degree of unsaturation [24].

Over the years, a number of area per lipid data have been published for the various headgroup-containing (e.g. PC, PG, PE, etc.) lipids found in nature (e.g. [7,9,12,25–34]). However, the recent interest in MD simulations requires for systematic and more precise descriptions of the most commonly used lipids. The present work evaluates the molecular area of PC headgroup lipids with hydrocarbon chains of various length and degree of unsaturation, using the recently developed method for determining area per lipid described in Ref. [12]. In addition to lipid areas, a comprehensive list of other structural parameters is reported for lipid bilayers in the liquid crystalline phase as a function of temperature.

2. Materials and methods

Synthetic saturated acyl chain phosphatidylcholines: 1,2-dilauroyl-*sn*-glycero-3-phosphatidylcholine (diC12:0PC, DLPC), 1,2-dimyristoyl-*sn*-glycero-3-phosphatidylcholine (diC14:0PC, DMPC), 1,2-dipalmitoyl-*sn*-glycero-3-phosphatidylcholine (diC16:0PC, DPPC), 1,2-distearoyl-*sn*-glycero-3-phosphatidylcholine (diC18:0PC, DSPC), mixed acyl chain phosphatidylcholines: 1-palmitoyl-2-oleoyl-*sn*-glycero-3-phosphatidylcholine (C16:0–18:1PC, POPC) and 1-stearoyl-2-oleoyl-*sn*-glycero-3-phosphatidylcholine (C18:0–18:1PC, SOPC), and branched acyl chain phosphatidylcholine: 1,2-diphytanoyl-*sn*-glycero-3-phosphatidylcholine (di4MEC16:0PC, DPhyPC) were purchased from Avanti Polar Lipids (Alabaster, AL) and used without further purification. Up to 60 mg of each lipid was mixed with 1.5 ml D_2O (99.9% pure, Chalk River Laboratories) or 18 MΩcm H_2O (Millipore), and temperature cycled through the main phase transition until a uniform dispersion of multilamellar vesicles (MLVs) was obtained. Unilamellar vesicles (ULVs) were then prepared from this dispersion at temperatures above the main phase transition of each lipid using an Avanti mini-extruder fitted with two 0.25 ml air-tight syringes. MLVs were extruded through two polycarbonate filters with pore diameters of 500 Å, producing ULVs with diameters ~600 Å [35]. The most "rigid" lipid (DSPC) was pre-extruded using two 2000 Å diameter filters to form large ULVs [36]. Finally, samples were diluted with D_2O or H_2O to the desired external contrast condition (i.e. 100%, 70% and 50% D_2O in the case of neutron contrast variation experiments, and 100% H_2O in the case of X-ray scattering experiments). The total lipid concentration of all ULV samples was ~20 mg/ml, guaranteeing sufficient water between ULVs and eliminating the possibility of any inter-particle interactions [35].

2.1. Small-angle X-ray scattering

X-ray data were taken at the Cornell High Energy Synchrotron Source (CHESS) G-1 station. A 1.18 Å wavelength (λ) incident X-ray beam of dimensions 0.24×0.24 mm^2 was detected using a 1024×1024 pixel array FLICAM charge-coupled device (CCD), with 69.78 μm linear dimension pixels. The sample-to-detector distance (SDD) was 423.6 mm, as determined using silver behenate (d-spacing of 58.367 Å). Samples were contained in 1.5 mm quartz capillaries placed in a temperature controlled, multi-position sample holder. 2D images were de-zingered using two consecutive 10 s exposures, and corrected using calibration files supplied by CHESS. Data sets were normalized using the incident beam intensity as measured by an ion chamber. Background scattering resulting from water and air scatter was subtracted according to the procedure

described in Ref. [35]. An additional linear function was used to correct for an unaccountable rise in background scattering similar to Ref. [37], while the use of an absorption correction was found unnecessary (see Appendix A). A typical curve of scattering form factors determined by

$$F(q) = \sqrt{I(q)q^2} \quad (1)$$

is shown in Fig. 1A.

2.2. Small-angle neutron scattering

Neutron scattering data were taken at the NG-3 and NG-7 stations [38] located at the National Institute of Standards and Technology (NIST) Center for Neutron Research (NCNR), and at the CG-3 Bio-SANS instrument [39] located at the Oak Ridge National Laboratory (ORNL) Center for Structural Molecular Biology (CSMB). 6 Å wavelength neutrons were selected using a mechanical velocity selector, with an energy dispersion of 12.5, 11.5 and 14.5% (FWHM), respectively. Multiple sample-to-detector distances (i.e. 1.3, 5 and 13.2 m at NG-3; 2, 5 and 15.3 m at NG-7; 2.5 and 15.3 m at CG-3) were used, resulting in a total scattering vector [$q = 4\pi/\lambda \sin(\theta)$, where λ is the wavelength and 2θ is the scattering angle] of $0.003 < q < 0.3$ Å^{-1}. Data were collected using two-dimensional ^{3}He position-sensitive detectors with a 5 mm × 5 mm resolution (640 × 640 mm^2 at NIST, and a 1 × 1 m^2 at ORNL). Samples were taken up in standard 1 mm path length quartz (banjo) cells. Finally, acquired 2D images were corrected and reduced into 1D scattering curves using software supplied by NIST [40] and ORNL, and no absorption correction was applied (see Appendix A). Fig. 1B shows typical neutron scattering form factors calculated using Eq. (1).

2.3. Bilayer model

The SDP model was developed by Ref. [12] and is graphically depicted in Fig. 1C–E. Briefly, the component groups are chosen on the basis that each group has the same functional form for all the different contrast conditions [i.e. X-ray (Fig. 1C) and neutron (Fig. 1D) scattering density profiles]. For example, carbonyl and glycerol groups are described by a single Gaussian (CG), the phosphate and part of the choline (CH_2CH_2N) by another Gaussian (PCN), and the remaining choline ($3xCH_3$) by yet another Gaussian ($CholCH_3$). In effect, three Gaussians are used to describe the PC headgroup. The error function represents the total hydrocarbon region (i.e. sum of CH_2, CH and CH_3 groups). CH and CH_3 groups are each described by a single Gaussian, which are then subtracted from the error function to obtain the CH_2 distribution. The water distribution is not defined by any particular function, but is instead calculated based on the complementarity requirement, whereby all of the probabilities add up to one. In this way the model captures all of the features of the different scattering density profiles (SDPs) while satisfying the spatial conservation principle. Therefore, the volume probabilities (Fig. 1E) of the component groups in the SDP model sum up to unity at each point z along the bilayer normal [12].

From Fig. 1 it is obvious that neutrons and X-rays are sensitive to different parts of the bilayer. For example, in the case of X-rays the electron dense phosphate groups contrast very well with the less electron dense hydrocarbon region. Thus, X-ray data are well suited for the refinement of the lipid headgroup and hydrocarbon chains. On the other hand, the high neutron scattering length density of D_2O (often used in neutron experiments instead of H_2O in order to increase the scattering contrast between the bilayer and the solvent, and to reduce background) permits neutron scattering to accurately determine the total bilayer thickness, and consequently, lipid area. Based on the amount and the quality of the experimental data included in the analysis, we estimate the uncertainty of the various structural parameters to be about 2% [34].

Although the SDP model is designed to obtain structure from X-ray and neutron scattering data, the primary description is in terms of volume probability distributions (Fig. 1E). Lipid area A then follows from the volume probability of the water distribution, which gives the Gibbs dividing surface between the water and the lipid. In particular, the mean position of the water distribution is defined by the equality of the integrated water probabilities to the left of the Gibbs dividing surface and the integrated deficit of water probabilities to its right (see hatched areas in Fig. 1E). In other words, the Gibb's dividing surface is equivalent to Luzzati's division of two component systems consisting of water and lipid [11].

3. Results

X-ray scattering form factors for the different lipid bilayers studied were measured in H_2O, while neutron scattering form factors were determined at three different contrast conditions (i.e. 100, 70 and 50% D_2O). These bilayers were measured at four different temperatures (i.e.

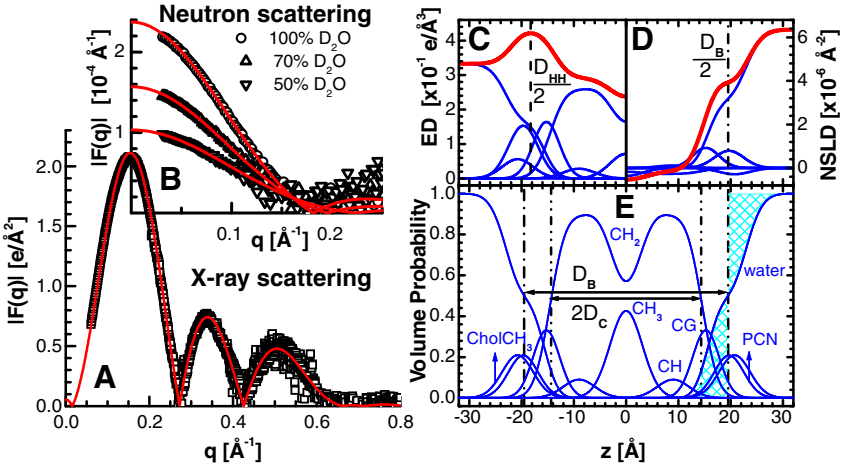

Fig. 1. An illustration of lipid bilayer structure determination through the simultaneous analysis of X-ray and neutron scattering data obtained from POPC bilayers at 30 °C. Graphs on the left show the experimental X-ray (A) and contrast varied neutron (B) scattering form factors (points), together with the best fits to the data (solid lines). The scattering density profile (SDP) model of a bilayer in real space is shown on the right, where the top panels show electron densities (ED) (C) and neutron scattering length densities (NSLD) (D) of the various lipid component distributions, including the total scattering density (thick lines). Panel (E) shows volume probability distributions, where the total probability is equal to 1 at each point across the bilayer. The definition of the Gibb's dividing surface is demonstrated for the interface between the lipid bilayer and the water phase (effectively D_B) — a point on the z axis where the integrated areas (hatched) are equal.

20, 30, 50 and 60 °C), which in the case of some lipids covered both gel (data not shown) and liquid–crystalline phases. As a function of increasing temperature, the bilayer structural parameters, which depend on the interplay between increasing lipid volume [volume thermal expansivity: $\alpha_V = (1/V)(\partial V/\partial T)_{\Pi}$, where Π suggests a constant pressure], increasing lipid area [area thermal expansivity: $\alpha_A = (1/A)(\partial A/\partial T)_{\Pi}$)], and decreasing bilayer thickness [thickness thermal contractivity: $\alpha_D = -(1/D)(\partial D/\partial T)_{\Pi}$], changed linearly. Thermal coefficients are determined from the slopes of the linear functions used to fit the various temperature dependent data. Uncertainties are estimated from the chi-squares, and include both the variance due to the assigned uncertainties and the weighted squares of the residuals, i.e.

$$\chi^2 = \frac{1}{\sum_n 1/\sigma_i^2} + \frac{\sum_n 1/\sigma_i^2 [y_i - (kx_i + c)]^2}{n-2}, \quad (2)$$

where σ_i is the uncertainty of parameter y_i at point x_i, and k and c are the coefficients of the linear function. This way, the fits to the data with the fewest number of points also possess the largest uncertainties.

3.1. 1,2-dilauroyl-sn-glycero-3-phosphatidylcholine (diC12:0PC, DLPC)

The thickness and lipid area of DLPC bilayers as a function of temperature are given in Fig. 2. They were obtained through the simultaneous analysis of X-ray and neutron ULV data. In the case of 30 °C bilayers, ULV neutron and X-ray scattering form factors were refined using X-ray data previously obtained from stacks of oriented (ORI) bilayers [41]. In doing so, we are able to further evaluate the robustness of our method. While ULV data provide the strongest scattering signal at the low and mid q range, ORI samples allow us to extend the form factors up to $q = 0.82$ Å^{-1}, thus increasing the resolution of our real space reconstruction. Bilayer profiles obtained from these two approaches (see Figs. S1 and S3 in the Supplementary material) show that the largest differences are observed in the widths of the terminal methyl groups. However, it is obvious from Fig. 2 that the inclusion of the ORI data did not alter area/lipid or the thickness of DLPC bilayers at 30 °C.

The gel-to-fluid transition temperature of DLPC at ~−1 °C [24,25,42] is well below the range of temperatures examined in this study, placing all of our DLPC bilayers (i.e. 20, 30, 50 and 60 °C) well into the fluid phase. All the scattering form factors are consistent with fluid phase bilayers (see the Supplementary material) and show only small variations with changing temperature. These variations correspond to the linear changes taking place due to increasing lipid volume and area/lipid as a function of increasing temperature, and the concomitant decrease in bilayer thickness. From the slopes of the structural data plotted as a function of temperature (Fig. 2), the corresponding thermal coefficients are determined and are listed in Tables 1–3 (see also Table S1 for detailed results).

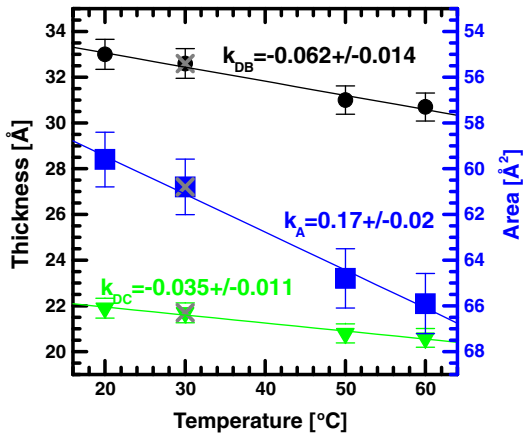

Fig. 2. Temperature dependence of DLPC bilayer thickness (black circles represent D_B, and green triangles represent $2D_C$) and lipid area (blue squares). For the most part, the data shown are from the analysis of ULVs, while values denoted by the gray X symbols (30 °C) are from the joint refinement of ULV and ORI samples.

3.2. 1,2-dimyristoyl-sn-glycero-3-phosphatidylcholine (diC14:0PC, DMPC)

The thickness and lipid area of DMPC bilayers as a function of temperature are given in Fig. 3 (also Tables 1–3). Similar to what was done with DLPC bilayers (Fig. 2), the ULV neutron and X-ray scattering form factors were reanalyzed using X-ray data previously obtained from ORI stacks of DMPC bilayers at 30 °C [41]. Although the scattering statistics are again improved in the high q region (see Fig. S6 in Supplementary material), the resulting bilayer parameters differ negligibly whether or not ORI data are used (Fig. 3).

The gel-to-fluid transition temperature for DMPC bilayers is reported to be between ~23 and ~24 °C [14,24,25,42]. As a result, we only have three liquid crystalline DMPC bilayer data sets (Fig. 3). The thermal thickness contractivity and area expansivity are evaluated from the slopes of the linear fits to the data (Fig. 3). A complete list of bilayer structural parameters for liquid crystalline DMPC bilayers can be found in Table S2 of the Supplementary materials section.

3.3. 1,2-dipalmitoyl-sn-glycero-3-phosphatidylcholine (diC16:0PC, DPPC) and 1,2-distearoyl-sn-glycero-3-phosphatidylcholine (diC18:0PC, DSPC)

DPPC and DSPC have main transition temperatures of ~41–42 °C and ~54–55 °C, respectively [14,24,25,42,43]. Thus we only collected two sets of liquid crystalline data of DPPC bilayers and one set of DSPC bilayers. In the case of DPPC, previously obtained X-ray ORI data from liquid crystalline bilayers at 50 °C [12] are analyzed for comparison — similar to what was done for DLPC and DMPC bilayers. Although the inclusion of the ORI data affects the scattering form factors in the higher q region (compare Figs. S10 and S11), the differences in real space data are again negligible (Fig. 4).

The various bilayer thicknesses and lipid areas for liquid crystalline DPPC and DSPC bilayers, as a function of temperature, are shown in Fig. 4 and Tables 1–3. The thermal thickness contractivity and area expansivity are evaluated from the slopes of the linear fits to the DPPC data, only. A complete list of bilayer structural parameters for liquid crystalline DPPC and DSPC bilayers can be found in Table S3 of the Supplementary materials section.

3.4. 1-palmitoyl-2-oleoyl-sn-glycero-3-phosphatidylcholine (C16:0–18:1PC, POPC)

POPC bilayers undergo a gel-to-liquid crystalline phase transition around −2 °C [43]. As such, all of the data shown in Fig. 5 are of liquid crystalline POPC bilayers. It is interesting to note the decreased number of lobes observed in the X-ray scattering form factors at 30 °C (see Fig. S14 of the Supplementary materials). Although the ORI data are available up to $q = 0.8$ Å^{-1}, they are essentially of zero amplitude beyond $q = 0.6$ Å^{-1} — the result of a rather smooth scattering density profile with no discernable real space features smaller than 10 Å. In many ways this result justifies the use of analyzing only ULV data which cover the entire range of useful scattering. Not surprisingly, there are virtually no differences between the two results (i.e. ULV data vs. combined ULV and ORI data) shown in Fig. 5.

We had some difficulty in fitting the 20 °C POPC X-ray scattering form factors (see Fig. S15 of the Supplementary material), but the fits to the remaining data were excellent. Moreover, the temperature dependence

Table 1
Lipid area (A), thermal area expansivity ($\alpha_A^T = (1/A)(\partial A/\partial T)_{\Pi}$), and area expansivity as a function of hydrocarbon chain length ($\alpha_A^n = (1/A)(\partial A/\partial n)_{\Pi}$) for the various fluid bilayers studied. The uncertainties (+/−) shown below the main values are calculated according to Eq. (2).

	20 °C			30 °C			50 °C			60 °C		
	A [Å^2]	α_A^T [deg^{-1}]	α_A^n	A [Å^2]	α_A^T [deg^{-1}]	α_A^n	A [Å^2]	α_A^T [deg^{-1}]	α_A^n	A [Å^2]	α_A^T [deg^{-1}]	α_A^n
DLPC	59.6	0.0029	N/A	60.8	0.0028	−0.0074	64.8	0.0026	−0.0066	65.9	0.0026	−0.0053
	1.2	0.0007		1.2	0.0007	0.0100	1.3	0.0006	0.0093	1.3	0.0006	0.0025
DMPC	Gel			59.9	0.0032	−0.0075	63.3	0.0030	−0.0068	65.7	0.0029	−0.0053
				1.2	0.0007	0.0102	1.3	0.0007	0.0096	1.3	0.0007	0.0025
DPPC	Gel			Gel			63.1	0.0030	−0.0068	65.0	0.0029	−0.0054
							1.3	0.0021	0.0096	1.3	0.0020	0.0026
DSPC	Gel			Gel			Gel			63.8	N/A	−0.0055
										1.3		0.0026
POPC	62.7	0.0022	0.018	64.3	0.0022	0.019	67.3	0.0021	0.012	68.1	0.0021	0.019
	1.3	0.0004	0.022	1.3	0.0004	0.021	1.3	0.0003	0.021	1.4	0.0003	0.021
SOPC	63.8	0.0022	0.017	65.5	0.0021	0.018	68.1	0.0021	0.012	69.4	0.0020	0.019
	1.3	0.0004	0.020	1.3	0.0003	0.020	1.4	0.0003	0.021	1.4	0.0003	0.021
DPhyPC	78.0	0.0019	N/A	80.6	0.0019	N/A	83.6	0.0018	N/A	84.8	0.0018	N/A
	1.6	0.0004		1.6	0.0004		1.7	0.0004		1.7	0.0004	

data of POPC bilayer structural features, shown in Fig. 5, are consistent with the data obtained from the other bilayers studied (Figs. 2–4).

3.5. 1-stearoyl-2-oleoyl-sn-glycero-3-phosphatidylcholine (C18:0–18:1PC, SOPC)

Compared to POPC bilayers, SOPC bilayers have a slightly higher main transition temperature i.e. ~6 °C [43]. Liquid crystalline SOPC bilayers were studied at four different temperatures and the structural data resulting from the SDP analysis are shown in Fig. 6. Similar to the data already presented, D_B and D_C decrease linearly as a function of temperature, while values for A increase. The data are shown in Tables 1–3.

Similar to the POPC data, 20 °C SOPC X-ray scattering form factors show a small "lift off" in the two low-q minima (see Fig. S20 of Supplementary material). The observation of non-zero minima is indicative of an asymmetric bilayer scattering profile [44]. Although single lipid bilayers are expected to be symmetric in the fluid phase, it is possible that lipids with longer and stiffer hydrocarbon chains are more prone to forming asymmetric bilayers when close to their melting temperature. Overall, this asymmetry is minor, and is only seen in the X-ray and not the neutron scattering form factors.

3.6. 1,2-diphytanoyl-sn-glycero-3-phosphatidylcholine (di4MEC16:0PC, DPhyPC)

DPhyPC is a lipid with branched hydrocarbon chains (3,7,11,15-tetramethylhexadecanoic). Compared to unsaturated hydrocarbon chain lipids, DPhyPC's saturated chains are less susceptible to photo-oxidation and degradation, yet it readily forms biologically relevant fluid phase bilayers [45]. DPhyPC's gel-to-fluid phase transition temperature is thought to be around −120 °C [46], thus all of our measurements were conducted on liquid crystalline bilayers (Fig. 7).

DPhyPC experimental data were easily fit using the SDP model (see Figs. S24–S28 in the Supplementary material). Similar to the other results presented here, data were obtained using ULVs, while previous X-ray data from ORI samples [47] were included in the case of 30 °C — as was done for some of the other bilayers. The inclusion of ORI data is in excellent agreement with structure data obtained from ULVs only (Fig. 7). The most pronounced differences between ULV data and ULV

Table 2
Bilayer thickness (D_B), its thermal contractivity ($\alpha_{DB}^T = -(1/D_B)(\partial D_B/\partial T)_{\Pi}$), and the contractivity as a function of hydrocarbon chain length ($\alpha_{DB}^n = -(1/D_B)(\partial D_B/\partial n)_{\Pi}$) for the various fluid bilayers studied. The uncertainties (+/−) shown below the main values are calculated according to Eq. (2).

	20 °C			30 °C			50 °C			60 °C		
	D_B [Å]	α_{DB}^T [deg^{-1}]	α_{DB}^n	D_B [Å]	α_{DB}^T [deg^{-1}]	α_{DB}^n	D_B [Å]	α_{DB}^T [deg^{-1}]	α_{DB}^n	D_B [Å]	α_{DB}^T [deg^{-1}]	α_{DB}^n
DLPC	33.0	0.0019	N/A	32.6	0.0019	0.064	31.0	0.0020	0.065	30.7	0.0020	0.062
	0.7	0.0008		0.7	0.0008	0.010	0.6	0.0009	0.008	0.6	0.0009	0.005
DMPC	Gel			36.7	0.0022	0.057	35.2	0.0023	0.057	34.2	0.0024	0.056
				0.7	0.0006	0.009	0.7	0.0006	0.007	0.7	0.0007	0.004
DPPC	Gel			Gel			39.0	0.0023	0.051	38.1	0.0024	0.050
							0.8	0.0021	0.006	0.8	0.0022	0.004
DSPC	Gel			Gel			Gel			42.2	N/A	0.045
										0.84		0.003
POPC	39.8	0.0014	0.025	39.1	0.0014	0.023	37.9	0.0014	0.029	37.7	0.0014	0.021
	0.8	0.0004	0.021	0.78	0.0004	0.021	0.8	0.0004	0.022	0.8	0.0004	0.021
SOPC	40.8	0.0014	0.025	40.0	0.0014	0.023	39.0	0.0014	0.028	38.5	0.0015	0.021
	0.8	0.0004	0.021	0.8	0.0004	0.021	0.8	0.0004	0.021	0.8	0.0004	0.021
DPhyPC	36.3	0.0011	N/A	35.4	0.0011	N/A	34.7	0.0011	N/A	35.2	0.0011	N/A
	0.7	0.0004		0.7	0.0004		0.7	0.0004		0.7	0.0004	

Table 3
Hydrocarbon region thickness ($2D_C$), its thermal contractivity ($\alpha^T_{DC} = -(1/D_C)(\partial D_C/\partial T)_{n}$), and the contractivity as a function of hydrocarbon chain length ($\alpha^n_{DC} = -(1/D_C)(\partial D_C/\partial n)_{T}$) for various fluid bilayers studied. The uncertainties (+/−) shown below the main values are calculated according to Eq. (2).

	20 °C			30 °C			50 °C			60 °C		
	$2D_C$ [Å]	α^T_{DC} [deg^{-1}]	α^n_{DC}	$2D_C$ [Å]	α^T_{DC} [deg^{-1}]	α^n_{DC}	$2D_C$ [Å]	α^T_{DC} [deg^{-1}]	α^n_{DC}	$2D_C$ [Å]	α^T_{DC} [deg^{-1}]	α^n_{DC}
DLPC	21.9	0.0016	N/A	21.7	0.0016	0.092	20.8	0.0017	0.091	20.6	0.0017	0.092
	0.4	0.0012		0.4	0.0012	0.011	0.4	0.0012	0.007	0.4	0.0012	0.007
DMPC	Gel			25.7	0.0020	0.078	24.8	0.0021	0.077	24.1	0.0022	0.079
				0.5	0.0007	0.009	0.5	0.0008	0.006	0.5	0.0008	0.006
DPPC	Gel			Gel			28.5	0.0021	0.067	27.9	0.0022	0.068
							0.6	0.0021	0.005	0.6	0.0022	0.005
DSPC	Gel			Gel			Gel			31.9	N/A	0.060
										0.6		0.004
POPC	29.2	0.0011	0.041	28.8	0.0011	0.038	28.1	0.0011	0.043	28.0	0.0011	0.036
	0.6	0.0004	0.021	0.6	0.0004	0.022	0.6	0.0004	0.022	0.6	0.0004	0.022
SOPC	30.4	0.0011	0.039	29.9	0.0011	0.037	29.3	0.0012	0.041	29.0	0.0012	0.034
	0.6	0.0003	0.020	0.6	0.0003	0.021	0.6	0.0004	0.021	0.6	0.0004	0.021
DPhyPC	27.8	0.0010	N/A	27.2	0.0011	N/A	26.7	0.0011	N/A	26.6	0.0011	N/A
	0.6	0.0005		0.5	0.0006		0.5	0.0006		0.5	0.0006	

data combined with ORI data are observed in the high q region, where an extra lobe is seen in the scattering form factors that include the higher resolution ORI data (see Fig. S24). In real space, this affects the structural parameters that X-rays are especially sensitive to (i.e. D_{HH}), or those that correspond to finer bilayer details where increased spatial resolution is required (see Table S7 in the Supplementary material). Not surprisingly, the exclusion of the ORI data yields real space structural data of lower spatial resolution and/or decreased sensitivity to bilayer features especially discernable by X-ray scattering. An example of this is the small value of D_{H1} (the distance from the phosphate to the interface of the hydrocarbon region; i.e. $2D_{H1} = D_{HH} - 2D_C$) at 20 °C. We believe this value is most likely the result of an artifact of the analysis in that, it is rather insensitive to the intrabilayer parameters when high resolution ORI data are not taken into account. On the other hand, the neutron scattering data make the SDP analysis very robust when it comes to determining the overall bilayer structural parameters (see Fig. 7 and Tables 1–3).

4. Discussion and conclusions

It is well known that the bilayer structure formed by lipid aggregates is due to the hydrophobic effect [48], whereby non-polar molecules aggregate in such a fashion as to exclude water. Lipid bilayers thus form spontaneously and the area/lipid is determined by the balance between changes in entropy and enthalpy. As the lipid's hydrocarbon chains are unable to hydrogen bond with water, they disrupt the hydrogen bonding network between water molecules — the magnitude of this disruption is directly related to the length of the hydrocarbon chains [49]. Similarly, van der Waals attractive forces between the hydrocarbon tails that contribute to decreasing lipid area depend directly on lipid chain length. On the other hand, increase in lipid area is caused by the increased probability of trans–gauche isomerization that happens to increase with chain length [42] and temperature. As a result, the equilibrium area/lipid at the bilayer-water interface is dictated by the fine balance of the forces that minimize the system's total free energy. It is thus not surprising that lipids with different length hydrocarbon chains and degree of unsaturation form bilayers with different thicknesses and lipid areas — it is worth noting that rotational isomerization depends on the absolute temperature rather than a reduced lipid temperature, which has no effect on the lipid's first order main transition [9]. Importantly then, is that key membrane parameters used to describe lipid–lipid and lipid–protein interactions are compared at the same absolute temperature.

4.1. The effect of temperature on fluid bilayers

Not surprising, the bilayer structural parameters A, D_B, and D_C differ among the various lipids and also vary as a function of temperature. It

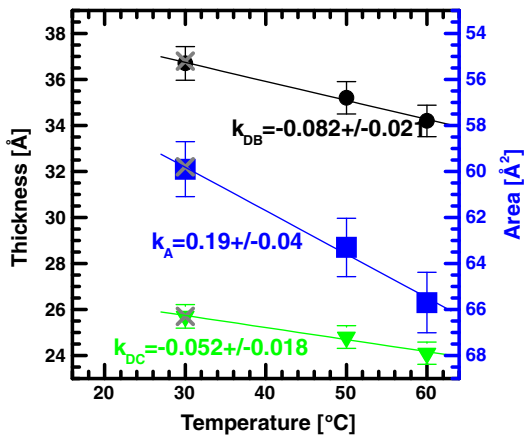

Fig. 3. Temperature dependence of DMPC bilayer thickness (black circles represent D_B, and green triangles represent $2D_C$) and area per lipid (blue squares). Data shown are from the analysis of ULVs, while data denoted by the gray X symbols (30 °C) are from the joint refinement of ULV and ORI samples.

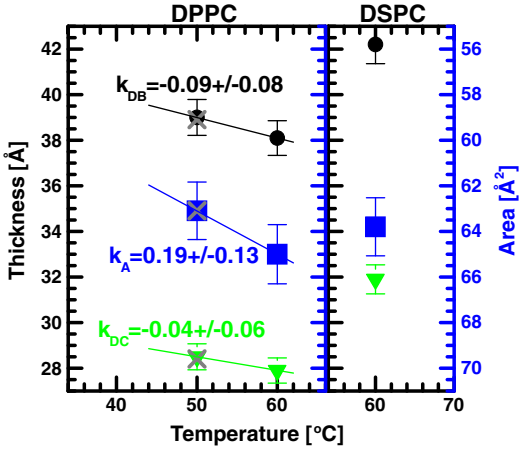

Fig. 4. Temperature dependence of liquid crystalline DPPC and DSPC bilayer thickness (black circles represent D_B, and green triangles represent $2D_C$) and lipid area (blue squares). Data shown are from the analysis of ULV samples, while data denoted by the gray X symbols (50 °C) are from the joint refinement of ULV and ORI DPPC samples.

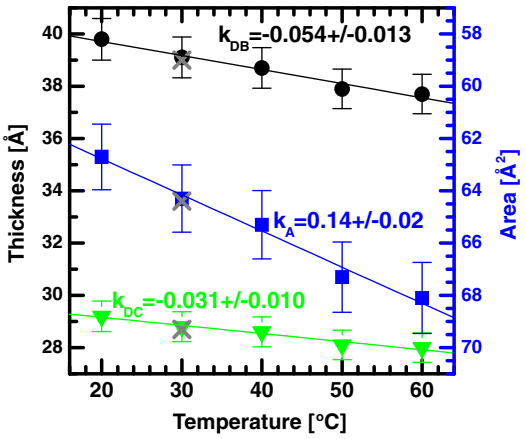

Fig. 5. Temperature dependence of liquid crystalline POPC bilayer thickness (black circles represent D_B, and green triangles represent $2D_C$) and lipid area (blue squares). Data shown are from the analysis of ULV samples, while data denoted by the gray X symbols (30 °C) are from the joint refinement of ULV and ORI samples.

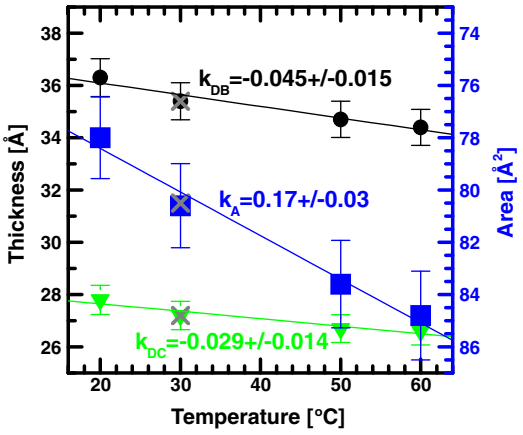

Fig. 7. Temperature dependence of liquid crystalline DPhyPC bilayer thickness (black circles represent D_B, and green triangles represent $2D_C$) and lipid area (blue squares). Data shown are from the analysis of ULVs, while data denoted by the gray X symbols (30 °C) are from the joint refinement of ULV and ORI samples.

is however reasonable to expect that these parameters vary with temperature in a similar fashion for all of the different lipids. The reason for this is that trans–gauche rotational isomerization has, among the other intrabilayer interactions, the strongest thermal dependence and affects, to a great extent, the thermal behavior of the various bilayer parameters. For example, the values for area thermal expansivity (α_A^T), bilayer thickness thermal contractivity (α_{DB}^T) and hydrophobic thickness thermal contractivity (α_{DC}^T) for the different lipids show only a small temperature dependence (see Tables 1–3). This is a result of our analysis having being performed well away from each lipid's gel phase (i.e. deep into the fluid phase). Near the phase transition temperature, however, there are significant subcritical bilayer fluctuations taking place (e.g. [50–52]) that can evoke more substantial temperature dependencies.

The experimental uncertainties were evaluated by considering two contributions, that of the expressed structural parameter itself, as well as the linear function's slope uncertainty that was used to fit that particular parameter (see Figs. 2–7). As a result, the fits to data with the fewest number of experimental points (e.g. temperature dependence of DPPC) contain the largest uncertainties (see Eq. (2)). Despite these uncertainties the temperature dependencies of the evaluated structural parameters suggest some interesting behavior. It seems that in terms of

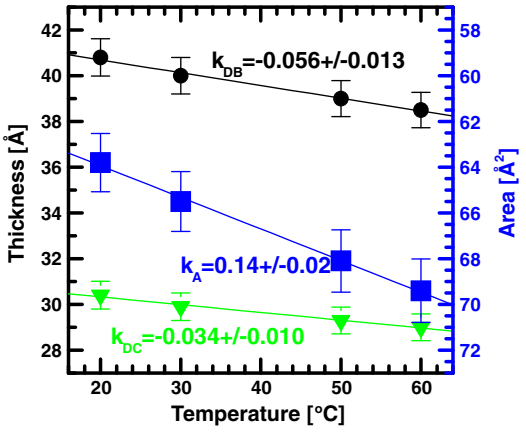

Fig. 6. Temperature dependence of the bilayer thickness (black circles represent D_B, and green triangles represent $2D_C$) and lipid area (blue squares) of liquid crystalline ULV SOPC bilayers.

increased lipid area due to increased temperature (i.e. k_A in Figs. 2–7), disaturated chain lipids (i.e. DLPC, DMPC, DPPC, and DSPC) behave similarly, while the addition of methyl groups (i.e. DPhyPC) to hydrocarbon chains alters their behavior noticeably. However, an even larger effect is caused by the addition of a double bond (i.e. POPC and SOPC). This observed decreased temperature dependence of a bilayer's area/lipid can be attributed to the existing disorder caused by multiple methyl groups or a double bond contributing significantly to an enhancement of thermal fluctuations with increasing temperature. Similar behavior has been observed by coarse-grained MD simulations. For example, the inclusion of one double bond decreased the $k_A = \Delta A/\Delta T$ slope by almost 30% [53], in good agreement with our value of ~26%.

In comparing our present results with previously published NMR data of saturated chain lipids [30] and X-ray results obtained from the di-monounsaturated DOPC lipid [33], previous data suggest that temperature has a much more pronounced effect on lipid area than observed in here. This discrepancy between the different studies can in part be attributed to differences in the absolute values of A, which seem to generally be larger when determined from standalone X-ray scattering experiments [12]. Nevertheless, our molecular area expansivity values k_A vary between 0.14 Å^2/deg for mixed chain lipids and 0.19 Å^2/deg for saturated lipids, in contrast to the 0.21 Å^2/deg value reported for DOPC by Pan et al. [33] and the ~0.27 Å^2/deg value reported for saturated lipids by Ref. [30]. Similarly, a larger lipid area expansivity for fluid DMPC bilayers was obtained by Needham and Evans [54] using giant ULVs and micropipette aspiration. However, Needham and Evans noted that their technique was sensitive to the apparent area of the vesicles and not the actual membrane area. Because of local membrane undulations present in stress-free giant ULVs, the apparent and true local areas may be different. Moreover, such undulations are affected by temperature and may be much more pronounced near the chain melting temperature [50–52]. On the other hand, our results are in good agreement with the X-ray measurements by Costigan et al. [55], where they determined $k_A = 0.21$ Å^2/deg and $\alpha_A^T = 0.0032$ deg^{-1} for DMPC bilayers.

4.2. The effect of hydrocarbon chain on fluid bilayers

Unlike the case where temperature only profoundly affects the probability of trans–gauche isomerization, changes to a lipid's hydrocarbon chain length can affect all of the above-discussed intrabilayer interactions (i.e. hydrophobic effect, van der Waals interactions, and trans–gauche isomerization). The equilibrium lipid area is then the result of the fine balance between all of these interactions. Interestingly,

our results suggest that there are differences between the chain length dependencies for saturated and mixed chain lipids. For example, at a given temperature a decrease in lipid area as a function of increased saturated fatty acid chain length is observed (Fig. 8a). This implies a smaller increase of the entropic contribution resulting from rotational isomerization (i.e. chain disorder), compared to the hydrophobic and van der Waals interactions in saturated chain lipids. In agreement with NMR [30] and simulations [53], our data imply that longer saturated hydrocarbon chains have an increasingly larger chain–chain van der Waals attractive energy, resulting in smaller lateral areas.

The situation, however, is dramatically different for lipids that contain one monounsaturated (oleoyl) fatty acid chain in the *sn*-2 position. Area/lipid increases upon the addition of two CH_2 groups for all temperatures studied (Fig. 8a). It is worth noting that this increase is about 3 times larger than the decrease we observed with saturated chain lipids, clearly demonstrating the importance that chain disorder has on area/lipid. In addition, compared to fully saturated chain lipid bilayers, bilayers formed by lipids with one monounsaturated chain (as well as those having two monounsaturated chains; [34]) exhibit larger areas/lipid at each of the given temperatures (Table 1 and Fig. 8a). The bilayer thicknesses, on the other hand (Tables 2 and 3, and Fig. 8b and c), are comparable to bilayers made of medium length saturated hydrocarbon chains, such as DPPC. This may be explained in terms of the *cis*-double bond perturbing the hydrocarbon chain packing. This is known to have a greater effect in lowering the main transition temperature than, for example, decreasing the length of the fatty acid chains [56]. Importantly, the extent of bilayer perturbation is known to depend on the double bond's position along the hydrocarbon chain, and is most pronounced when placed in the middle of the hydrocarbon chain [34,56].

An effect similar to the addition of a *cis*-double bond on bilayer transition temperature and bilayer structural properties (i.e. increased chain disorder and area per lipid) can be achieved by methyl substitution — also depends on where along the fatty acid chain the methyl group is placed [56]. In the case of DPhyPC that contains four methyl groups along each of its hydrocarbon chains, we observe an approximate 20 Å^2 increase in area per lipid (see Fig. 9). Also, for a given temperature DPhyPC's chains are between 3 and 4 Å shorter than DPPC's (see Tables 1–3). These intrinsic properties of DPhyPC bilayers have previously raised the question regarding its suitability in biophysical studies [47]. We extend this discussion by reporting on DPhyPC's thermal coefficients. Although the area expansivity α_A^T is the smallest of all of the lipids studied here, this can be attributed to the much larger area/lipid rather than the weaker temperature dependence. A comparison of molecular area expansivities k_A suggests that the thermal dependence for trans–gauche isomerization experienced by DPhyPC bilayers is in-between bilayers made of saturated chain lipids and those comprised of mixed chain lipids (see Figs. 2–7). The data presented here may thus aid in clarifying DPhyPC's suitability for biomimetic studies.

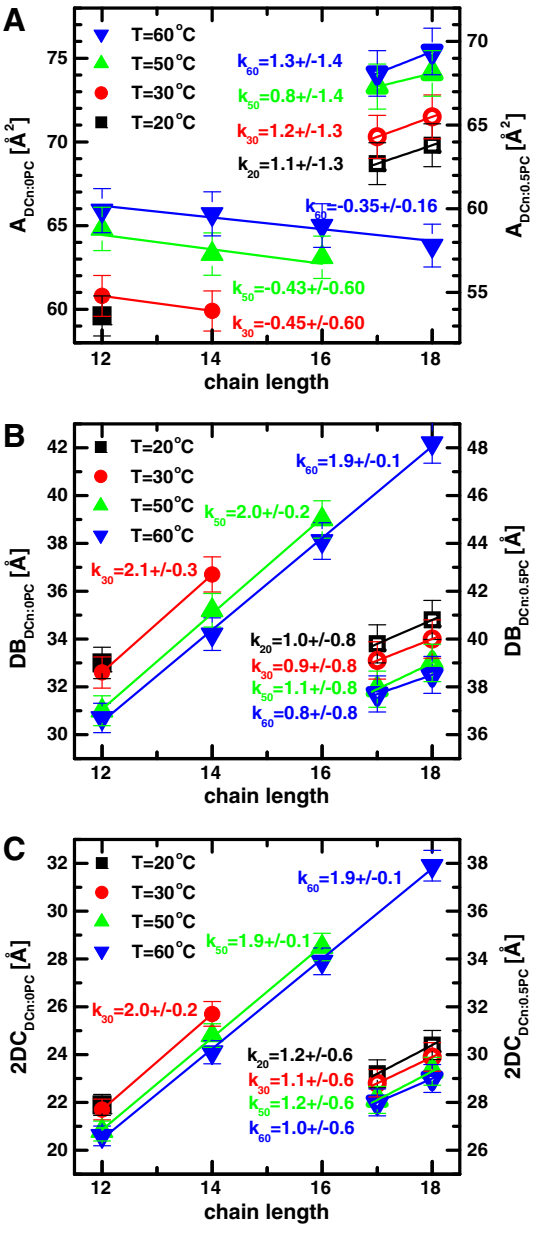

Fig. 8. The effect of hydrocarbon chain length on lipid area (A), bilayer thickness (B) and hydrocarbon chain thickness (C) for saturated fatty acid chain lipids (solid symbols) and mixed chain lipids (open symbols) at four different temperatures. Data from saturated chain and mixed chain lipids have been offset (y-axis) for clarity of presentation.

4.3. Lipid area in fluid bilayers

Fig. 9 summarizes areas/lipid for the various fluid bilayers at 30 °C. Note that the data points for lipids with higher transition temperatures (i.e. DPPC and DSPC) were extrapolated from fluid phase values using the appropriate thermal coefficients for area expansion (Tables 1–3).

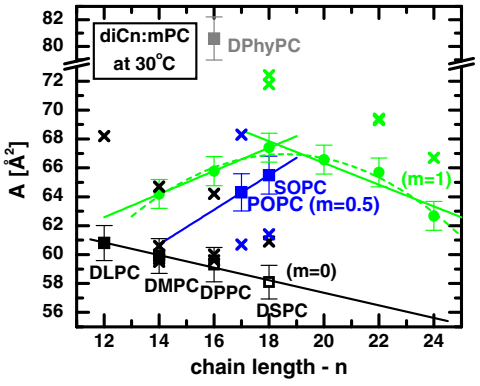

Fig. 9. Summary of area/lipid vs. hydrocarbon chain length for the various lipids studied at 30 °C. In the case of m = 0 (black squares), the fatty acid chains are fully saturated, while m = 0.5 (blue squares) and m = 1 (green circles) denote the presence of one and two monounsaturated fatty acid chains, respectively. The area/lipid for the branched fatty acid DPhyPC lipid is indicated by the gray square. All areas denoted by solid symbols (i.e. squares and circles) are obtained using 30 °C data, while areas indicated by open squares are calculated from fluid phase data using the determined thermal area expansivities. Squares (both open and solid) correspond to current data, while solid circles are from previously published lipid areas that were determined using the SDP analysis [34]. Xs represent lipid areas from literature (see the text for references). When needed, the averaged molecular area expansion $k_A = 0.167$ Å^2/deg was used to extrapolate the literature data to 30 °C.

This method of analysis reiterates the notion that such comparisons should be carried out at the same absolute temperature. Importantly, the evidence for an extended linear dependence of areas as a function of chain length corroborates our previous statement that, in the case of saturated fatty acid liquid crystalline PC bilayers, van der Waals forces are the determining factor of lateral lipid area.

The data depicted in Fig. 9 also reveals the effect that fatty acid unsaturation has on lipid area. As discussed, the presence of a *cis*-double bond perturbs the packing of the hydrocarbon chains, which results in increased chain disorder and a concomitant increase in lipid lateral area. Interestingly, the addition of two methylene groups to mixed chain lipids results in an increased area/lipid (blue symbols in Fig. 9), in contrast to the decrease experienced by saturated hydrocarbon chain lipids (black symbols in Fig. 9). This again suggests that rotational isomerization has a much more pronounced effect on lipid areas of mixed chain lipid bilayers than attractive van der Waals interactions. However, this behavior changes with the position of the double bond along the fatty acid chain. Previously published data by Kučerka et al. [34] showed both increasing and decreasing lipid lateral areas in di-monounsaturated PCs (green symbols in Fig. 9). This nonlinear behavior was explained in terms of double bond position. Lipids with double bonds fixed relative to the methyl terminus (i.e. $\omega 10$) can be fitted with a negative slope linear function — similar to that for saturated lipids. On the other hand, lipids with the double bonds fixed with respect to the PC headgroup (i.e. 9-*cis*) are fitted with a positive slope linear function — similar to the mixed chain lipids (with 9-*cis* double bond) reported here. From this we can conclude that bilayer thermodynamics for unsaturated lipids are determined by the double bond's position.

Comparing our current results of saturated and mixed chain lipids with previously reported areas for di-monounsaturated lipids [34], one can easily appreciate the profound effect that the first double bond has on lipid area. For example, of the increased area/lipid experienced by the substitution of two monounsaturated (e.g. *DOPC*) for two saturated (e.g. *DSPC*) fatty acid chains of same length, the addition of the first monounsaturated chain (e.g. *POPC*) accounts for between 70% and 80% of the increase. This result is in good agreement with a previous X-ray study that reported a 68% increase in area/lipid after the introduction of the first monounsaturated fatty acid chain [32].

We also compared our area/lipid values to previously published results. Lipid areas found in the literature vary considerably and depend, to a great extent, on the experimental technique used to obtain them. Substantial differences have been noted when utilizing standalone neutron and X-ray scattering data, compared to when they are jointly refined [12]. For example, DOPC's lipid area had been overestimated by about 10% when standalone X-ray data was used to determine its value. This can be seen in Fig. 9 whereby our present lipid areas are compared with some of the earlier results for di-monounsaturated chain lipid bilayers [25,33], mixed chain lipid bilayers [7,28,32], and fully saturated chain lipid bilayers [25]. As mentioned, the discrepancies are, for the most part, due to the utilization of limited data sets. It should also be pointed out that data for saturated lipid bilayers obtained from standalone X-ray scattering experiments [27,29] and/or NMR experiments [28,30] show much better agreement with our present results. Although the absolute areas/lipid are better obtained using our joint refinement method, perhaps a more important message is that the relative changes in lipid areas observed in the different bilayers (Fig. 9) seem to be consistent irrespective of the technique used to obtain them.

Area/lipid is often used as the key parameter when assessing the validity of MD simulations. Not unlike the disparate experimental results for lipid areas, published MD simulations (though not as numerous), have also resulted in a wide range of areas/lipid [57]. Consequently, many simulations have opted to fixing the area/lipid in order to achieve better agreement with experiment. Our present results can then enable this approach of simulating membrane structure and dynamics by providing them with the appropriate lipid area values, which have in turn been obtained utilizing models guided by simulation results. It is obvious, then, that this way of experimentally obtained lipid areas is also model dependent — as is the case here. It has been proposed that a good test for the validity of MD simulations is to compare them to experimentally obtained scattering density profiles [57]. However, even these are calculated based on certain assumptions. A better assessment of simulations is to compare them to "raw" experimental data (e.g. in form of scattering form factors), as suggested recently [58]. Our experimentally obtained scattering form factors shown in Figs. S1 to S28 thus again provide a basis for the synergy between experiment and simulation, whereby the simulation results guide the development of more realistic models, and experimental data aid in the development of more accurate MD force fields.

To conclude, we have determined a number of structural parameters pertaining to fluid phase bilayers of three different classes of PC bilayers, at a series of temperatures. Structural parameters such as area/lipid, bilayer thickness and hydrocarbon chain thickness were determined through the simultaneous analysis of small angle neutron and X-ray scattering data. Having determined accurate areas/lipid, we were then enabled to evaluate the lipid chain thermodynamics. Temperature was found to have the most profound effect with regard to rotational isomerizations for all lipids studied, while changes in hydrocarbon chain length affected bilayer dynamics differently for different lipids. Although chain disorder due to rotational isomerization still dominates in some of the unsaturated lipids, its influence is very much dependent on the double bond's position along the hydrocarbon chain. Finally, in the case of saturated hydrocarbon chain lipids, it is the attractive van der Waals chain–chain interactions that determine the area/lipid as a function of chain length.

Acknowledgments

This work acknowledges the support of the Office of Biological and Environmental Research at Oak Ridge National Laboratory's (ORNL) Center for Structural Molecular Biology (CSMB) through the utilization of facilities supported by the U.S. Department of Energy, managed by UT-Battelle, LLC under contract no. DE-AC05-00OR2275, facilities of the National Institute of Standards and Technology (NIST) supported in part by the National Science Foundation under agreement no. DMR-0944772, and the Cornell High Energy Synchrotron Source (CHESS), which is supported by the National Science Foundation and the National Institutes of Health/National Institute of General Medical Sciences under National Science Foundation award DMR-0225180. JK is partially supported by ORNL's Laboratory Directed Research and Development (LDRD) program.

Appendix A. Absorption correction

The use of an appropriate absorption correction is necessary when analyzing data from oriented (ORI) stacks of bilayers [37]. X-rays scattered at small q (proportional to θ as $\frac{4\pi}{\lambda}\sin\theta$) have, on average, longer path lengths within the ORI samples than those scattered at higher q, i.e. X-ray scattered at low q are absorbed more than X-rays scattered at higher q (Fig. A1a). The angular dependence of the absorption correction was calculated (Fig. A2) assuming a 10 μm thick sample with an absorption length $x_a = 2.5$ mm. Using this as our basis, the absorption at $q = 0.1$ Å^{-1} is almost 1.5 times greater than at $q = 1$ Å^{-1} (Fig. A2).

Similarly, the absorption correction can be evaluated for unilamellar vesicles (ULVs). However, the difference between the two sample geometries (i.e. ORI and ULV) is such that, for ULVs the path length, and thus the absorption factor, increases with the increasing q (see Fig. A1b). Quantitatively, absorption is expressed by the coefficient μ and is inversely proportional to the absorption length x_a. By definition, μdl is the attenuation of the beam through an infinitesimal sheet of

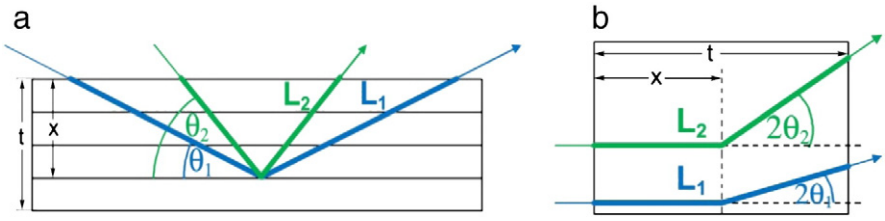

Fig. A1. Schematics of scattering geometries. (a) The reflection geometry utilized in ORI samples, and (b) the transmission geometry utilized in scattering from ULVs dispersed in water.

thickness dl at a path length l from the sample surface, which results in the scattering intensity expressed as [59]

$$I(l) = I_0 e^{-\mu l}. \tag{A1}$$

The path lengths for the two geometries shown in Fig. A1 are defined as

$$l_{reflection} = \frac{2x}{\sin\theta} \tag{A2a}$$

and

$$l_{transmission} = x + \frac{t-x}{\cos 2\theta}, \tag{A2b}$$

where x can assume any value from 0 up to the total sample thickness t. Eq. (A1) is then integrated along these path lengths over the entire thickness t. The resultant expression for the angular dependence of the scattered intensity due to sample absorption is then written as:

$$I_{reflection}(\theta) = I_0 \frac{x_a \sin\theta}{2t}\left(1 - \exp\left(-\frac{2t}{x_a \sin\theta}\right)\right) \tag{A3a}$$

and

$$I_{transmission}(\theta) = I_0 \frac{x_a \cos 2\theta}{t(\cos 2\theta - 1)} \exp\left(-\frac{t}{x_a \cos 2\theta}\right) \times\left(1 - \exp\left(-\frac{\cos 2\theta - 1}{x_a \cos 2\theta} t\right)\right). \tag{A3b}$$

The absorption correction is then applied to correct the experimentally measured scattering intensities.

Fig. A2 compares the normalized absorption corrections as a function of scattering vector q for typical X-ray scattering from ORI samples, X-ray scattering from ULVs, and neutron scattering from ULVs. It is obvious that the absorption correction is negligible in the case of ULVs.

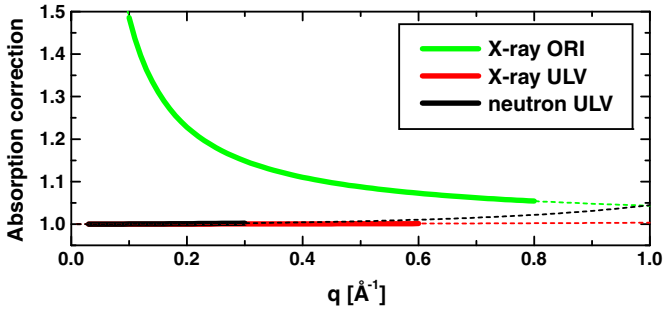

Fig. A2. Absorption corrections evaluated using Eqs. (A3a) and (A3b) for the scattering geometries described. X-ray scattering from ORI samples ($x_a = 2.5$ mm, $t = 0.01$ mm and $\lambda = 1.18$ Å) is measured in reflection geometry, while both X-ray ($x_a = 4$ mm, $t = 1.5$ mm and $\lambda = 1.18$ Å) and neutron ($x_a = 9.5$ mm, $t = 1$ mm and $\lambda = 6$ Å) scattering from ULV dispersions are measured in transmission geometry. Solid lines denote q-ranges that are typically accessible by the given experiment.

Appendix B. Supplementary data

Supplementary data to this article can be found online at doi:10.1016/j.bbamem.2011.07.022.

References

[1] A.G. Lee, How lipids affect the activities of integral membrane proteins, Biochim. Biophys. Acta 1666 (1–2) (2004) 62–87.
[2] P. Balgavý, J. Gallová, J. Karlovská, M. Kotalová, N. Kučerka, T. Murugova, J. Teixeira, D. Uhríková, Why and How to Measure Lipid Bilayer Thickness? in: Leon V. Berhardt (Ed.), Hauppauge, NY, 2010, pp. 439–450.
[3] J. Karlovská, D. Uhríková, N. Kučerka, J. Teixeira, F. Devínsky, I. Lacko, P. Balgavý, Influence of N-dodecyl-N, N-dimethylamine N-oxide on the activity of sarcoplasmic reticulum Ca(2+)-transporting ATPase reconstituted into diacylphosphatidylcholine vesicles: effects of bilayer physical parameters, Biophys. Chem. 119 (1) (2006) 69–77.
[4] T.A. Harroun, W.T. Heller, T.M. Weiss, L. Yang, H.W. Huang, Experimental evidence for hydrophobic matching and membrane-mediated interactions in lipid bilayers containing gramicidin, Biophys. J. 76 (2) (1999) 937–945.
[5] D.L. Worcester, N.P. Franks, Structural analysis of hydrated egg lecithin and cholesterol bilayers. II. Neutrol diffraction, J. Mol. Biol. 100 (3) (1976) 359–378.
[6] N. Kučerka, J.D. Perlmutter, J. Pan, S. Tristram-Nagle, J. Katsaras, J.N. Sachs, The effect of cholesterol on short- and long-chain monounsaturated lipid bilayers as determined by molecular dynamics simulations and X-ray scattering, Biophys. J. 95 (6) (2008) 2792–2805.
[7] G. Pabst, M. Rappolt, H. Amenitsch, P. Laggner, Structural information from multilamellar liposomes at full hydration: full Q-range fitting with high quality X-ray data, Phys. Rev. E Stat. Phys. Plasmas Fluids Relat. Interdiscip. Topics 62 (3 Pt B) (2000) 4000–4009.
[8] T.J. McIntosh, S.A. Simon, Hydration force and bilayer deformation: a reevaluation, Biochemistry 25 (14) (1986) 4058–4066.
[9] J.F. Nagle, S. Tristram-Nagle, Structure of lipid bilayers, Biochim. Biophys. Acta 1469 (3) (2000) 159–195.
[10] N. Kučerka, J.F. Nagle, S.E. Feller, P. Balgavý, Models to analyze small-angle neutron scattering from unilamellar lipid vesicles, Phys. Rev. E Stat. Nonlin. Soft Matter Phys. 69 (5 Pt 1) (2004) 051903.
[11] V. Luzzati, F. Husson, The structure of the liquid-crystalline phases of lipid–water systems, J. Cell Biol. 12 (2) (1962) 207–219.
[12] N. Kučerka, J.F. Nagle, J.N. Sachs, S.E. Feller, J. Pencer, A. Jackson, J. Katsaras, Lipid bilayer structure determined by the simultaneous analysis of neutron and X-ray scattering data, Biophys. J. 95 (5) (2008) 2356–2367.
[13] J.B. Klauda, N. Kučerka, B.R. Brooks, R.W. Pastor, J.F. Nagle, Simulation-based methods for interpreting X-ray data from lipid bilayers, Biophys. J. 90 (8) (2006) 2796–2807.
[14] J.F. Nagle, D.A. Wilkinson, Lecithin bilayers. Density measurement and molecular interactions, Biophys. J. 23 (2) (1978) 159–175.
[15] B.W. Koenig, K. Gawrisch, Specific volumes of unsaturated phosphatidylcholines in the liquid crystalline lamellar phase, Biochim. Biophys. Acta 1715 (1) (2005) 65–70.
[16] D. Uhríková, P. Rybár, T. Hianik, P. Balgavý, Component volumes of unsaturated phosphatidylcholines in fluid bilayers: a densitometric study, Chem. Phys. Lipids 145 (2) (2007) 97–105.
[17] D.M. Engelman, Surface area per lipid molecule in the intact membrane of the human red cell, Nature 223 (5212) (1969) 1279–1280.
[18] J.C. Mathai, S. Tristram-Nagle, J.F. Nagle, M.L. Zeidel, Structural determinants of water permeability through the lipid membrane, J. Gen. Physiol. 131 (1) (2008) 69–76.
[19] J.F. Nagle, J.C. Mathai, M.L. Zeidel, S. Tristram-Nagle, Theory of passive permeability through lipid bilayers, J. Gen. Physiol. 131 (1) (2008) 77–85.
[20] R.S. Cantor, Lateral pressures in cell membranes: a mechanism for modulation of protein function, J. Phys. Chem. B 101 (10) (1997) 1723–1725.
[21] R.W. Benz, F. Castro-Roman, D.J. Tobias, S.H. White, Experimental validation of molecular dynamics simulations of lipid bilayers: a new approach, Biophys. J. 88 (2) (2005) 805–817.
[22] C. Anezo, A.H. de Vries, H.D. Holtje, D.P. Tieleman, S.J. Marrink, Methodological issues in lipid bilayer simulations, J. Phys. Chem. B 107 (35) (2003) 9424–9433.
[23] J.N. Sachs, H.I. Petrache, T.B. Woolf, Interpretation of small angle X-ray measurements guided by molecular dynamics simulations of lipid bilayers, Chem. Phys. Lipids 126 (2) (2003) 211–223.

[24] P.R. Cullis, M.J. Hope, Physical Properties and Structural Roles of Lipids in Membranes, in: Dennis E. Vance, Jean E. Vance (Eds.), 1985, pp. 25–72.
[25] B.A. Lewis, D.M. Engelman, Lipid bilayer thickness varies linearly with acyl chain length in fluid phosphatidylcholine vesicles, J. Mol. Biol. 166 (2) (1983) 211–217.
[26] T.J. McIntosh, S.A. Simon, Area per molecule and distribution of water in fully hydrated dilauroylphosphatidylethanolamine bilayers, Biochemistry 25 (17) (1986) 4948–4952.
[27] J.F. Nagle, R. Zhang, S. Tristram-Nagle, W. Sun, H.I. Petrache, R.M. Suter, X-ray structure determination of fully hydrated L alpha phase dipalmitoylphosphatidylcholine bilayers, Biophys. J. 70 (3) (1996) 1419–1431.
[28] B.W. Koenig, H.H. Strey, K. Gawrisch, Membrane lateral compressibility determined by NMR and X-ray diffraction: effect of acyl chain polyunsaturation, Biophys. J. 73 (4) (1997) 1954–1966.
[29] H.I. Petrache, S. Tristram-Nagle, J.F. Nagle, Fluid phase structure of EPC and DMPC bilayers, Chem. Phys. Lipids 95 (1) (1998) 83–94.
[30] H.I. Petrache, S.W. Dodd, M.F. Brown, Area per lipid and acyl length distributions in fluid phosphatidylcholines determined by (2)H NMR spectroscopy, Biophys. J. 79 (6) (2000) 3172–3192.
[31] P. Balgavý, M. Dubničková, N. Kučerka, M.A. Kiselev, S.P. Yaradaikin, D. Uhríková, Bilayer thickness and lipid interface area in unilamellar extruded 1,2-diacylphosphatidylcholine liposomes: a small-angle neutron scattering study, Biochim. Biophys. Acta 1512 (1) (2001) 40–52.
[32] N. Kučerka, S. Tristram-Nagle, J.F. Nagle, Structure of fully hydrated fluid phase lipid bilayers with monounsaturated chains, J. Membr. Biol. 208 (3) (2005) 193–202.
[33] J. Pan, S. Tristram-Nagle, N. Kučerka, J.F. Nagle, Temperature dependence of structure, bending rigidity, and bilayer interactions of dioleoylphosphatidylcholine bilayers, Biophys. J. 94 (1) (2008) 117–124.
[34] N. Kučerka, J. Gallová, D. Uhríková, P. Balgavý, M. Bulacu, S.J. Marrink, J. Katsaras, Areas of monounsaturated diacylphosphatidylcholines, Biophys. J. 97 (7) (2009) 1926–1932.
[35] N. Kučerka, J. Pencer, J.N. Sachs, J.F. Nagle, J. Katsaras, Curvature effect on the structure of phospholipid bilayers, Langmuir 23 (3) (2007) 1292–1299.
[36] N. Kučerka, J. Pencer, M.P. Nieh, J. Katsaras, Influence of cholesterol on the bilayer properties of monounsaturated phosphatidylcholine unilamellar vesicles, Eur. Phys. J. E 23 (3) (2007) 247–254.
[37] Y. Liu, New Method to Obtain Structure of Biomembranes Using Diffuse X-Ray Scattering: Application to Fluid Phase DOPC Lipid Bilayers, Carnegie Mellon University, 2003.
[38] C.J. Glinka, J.G. Barker, B. Hammouda, S. Krueger, J.J. Moyer, W.J. Orts, The 30 m small-angle neutron scattering instruments at the National Institute of Standards and Technology, J. Appl. Cryst. 31 (1998) 430–445.
[39] W.T. Heller, G.W. Lynn, V.S. Urban, K. Weiss, D.A.A. Myles, The Bio-SANS small-angle neutron scattering instrument at Oak Ridge National Laboratory, Neutron News 19 (2) (2008) 22–23.
[40] S.R. Kline, Reduction and analysis of SANS and USANS data using IGOR Pro, J. Appl. Cryst. 39 (6) (2006) 895–900.
[41] N. Kučerka, Y. Liu, N. Chu, H.I. Petrache, S. Tristram-Nagle, J.F. Nagle, Structure of fully hydrated fluid phase DMPC and DLPC lipid bilayers using X-ray scattering from oriented multilamellar arrays and from unilamellar vesicles, Biophys. J. 88 (4) (2005) 2626–2637.
[42] G. Cevc, D. Marsh, Phospholipid bilayers, Phys. Princ. Models (5) (1987).
[43] Avanti Polar Lipids, http://www.avantilipids.com/ 2011.
[44] N. Kučerka, M.P. Nieh, J. Katsaras, Asymmetric distribution of cholesterol in unilamellar vesicles of monounsaturated phospholipids, Langmuir 25 (23) (2009) 13522–13527.
[45] Y. Wu, K. He, S.J. Ludtke, H.W. Huang, X-ray diffraction study of lipid bilayer membranes interacting with amphiphilic helical peptides: diphytanoyl phosphatidylcholine with alamethicin at low concentrations, Biophys. J. 68 (6) (1995) 2361–2369.
[46] H. Lindsey, N.O. Petersen, S.I. Chan, Physicochemical characterization of 1,2-diphytanoyl-Sn-glycero-3-phosphocholine in model membrane systems, Biochim. Biophys. Acta 555 (1) (1979) 147–167.
[47] S. Tristram-Nagle, D.J. Kim, N. Akhunzada, N. Kučerka, J.C. Mathai, J. Katsaras, M. Zeidel, J.F. Nagle, Structure and water permeability of fully hydrated diphytanoylPC, Chem. Phys. Lipids 163 (6) (2010) 630–637.
[48] C. Tanford, The Hydrophobic Effect: Formation of Micelles and Biological Membranes, John Wiley and Sons, New York, 1980.
[49] P. Yeagle, The Structure of Biological Membranes, in: Philip Yeagle (Ed.), CRC Press, Boca Raton, 1992.
[50] P.C. Mason, J.F. Nagle, R.M. Epand, J. Katsaras, Anomalous swelling in phospholipid bilayers is not coupled to the formation of a ripple phase, Phys. Rev. E Stat. Nonlin. Soft Matter Phys. 63 (3 Pt 1) (2001) 030902.
[51] G. Pabst, H. Amenitsch, D.P. Kharakoz, P. Laggner, M. Rappolt, Structure and fluctuations of phosphatidylcholines in the vicinity of the main phase transition, Phys. Rev. E Stat. Nonlin. Soft Matter Phys. 70 (2 Pt 1) (2004) 021908.
[52] N. Chu, N. Kučerka, Y. Liu, S. Tristram-Nagle, J.F. Nagle, Anomalous swelling of lipid bilayer stacks is caused by softening of the bending modulus, Phys. Rev. E Stat. Nonlin. Soft Matter Phys. 71 (4 Pt 1) (2005) 041904.
[53] M.J. Stevens, Coarse-grained simulations of lipid bilayers, J. Chem. Phys. 121 (23) (2004) 11942–11948.
[54] D. Needham, E. Evans, Structure and mechanical properties of giant lipid (DMPC) vesicle bilayers from 20 degrees C below to 10 degrees C above the liquid crystal-crystalline phase transition at 24 degrees C, Biochemistry 27 (21) (1988) 8261–8269.
[55] S.C. Costigan, P.J. Booth, R.H. Templer, Estimations of lipid bilayer geometry in fluid lamellar phases, Biochim. Biophys. Acta 1468 (1–2) (2000) 41–54.
[56] R.N.A.H. Lewis, R.N. McElhaney, in: Philip Yeagle (Ed.), The Mesomorphic Phase Behavior of Lipid Bilayers, CRC Press, Boca Raton, 1992, pp. 73–155.
[57] D. Poger, A.E. Mark, On the validation of molecular dynamics simulations of saturated and cis-monounsaturated phosphatidylcholine lipid bilayers: a comparison with experiment, J. Chem. Theory Comput. 6 (1) (2009) 325–336.
[58] N. Kučerka, J. Katsaras, J.F. Nagle, Comparing membrane simulations to scattering experiments: introducing the SIMtoEXP software, J. Membr. Biol. 235 (1) (2010) 43–50.
[59] J. Als-Nielsen, D. McMorrow, Elements of Modern X-Ray Physics, John Wiley & Sons, Ltd., 2001